Supporting Information

High-Temperature Variant of Oxygen-Rich Covalent Triazine Frameworks as Multifunctional Electrocatalysts

Ashish Kumar Maharana,[ab] Sourav Kumar Sarkar,[ab] Rahul Sarkar,[ab] Bibek Dash,[ab] Mrutyunjaya Majhi[ab] and Sanjib Das*[ab]

[a]Materials Chemistry & Interfacial Engineering Department, CSIR-Institute of Minerals & Materials Technology, Bhubaneswar 751013, India.

[b]Academy of Scientific and Innovative Research (AcSIR), Ghaziabad 201002, India.

Corresponding Author: sanjibdas.immt@csir.res.in

General information:

All chemical reagents were procured from reputable commercial sources and utilized as received unless specified otherwise.

Experimental measurements:

The crystallographic features of the samples were examined first by **powder X-ray diffraction** (PXRD) using a Rigaku Ultima-IV diffractometer equipped with monochromated Cu-Kα radiation (λ = 1.54060 Å); measurements were taken at 40 kV and 30 mA with a scan rate of 2° min^{-1} and a step size of 0.01° in 2θ. **Fourier-transform infrared** (FT-IR) spectra were then recorded over the 400-4000 cm^{-1} range using a Thermo Scientific Nicolet iS20 Smart iTX-Diamond ATR instrument. **Raman** analysis was performed with a Renishaw inVia confocal Raman microscope operated with a 532 nm diode laser. Morphological characterization was carried out by **field-emission scanning electron microscopy** (FE-SEM) on a JEOL JSM IT 800 SHL system, while **transmission electron microscopy** (TEM) imaging was conducted using a JEOL-JEM F200 microscope operated at 200 kV; for TEM, powdered samples were dispersed in ethanol and a drop of the suspension was deposited onto a carbon-coated copper grid. High-resolution **X-ray photoelectron spectroscopy** (XPS) was obtained using a Thermo Fisher Scientific ESCALAB Xi^+ spectrometer. **Gas adsorption and desorption** measurements up to 1 bar were performed on a Quantachrome Autosorb-iQ analyzer. Prior to analysis, samples were degassed under dynamic vacuum at 140 °C for 12 hours. Nitrogen adsorption isotherms at 77 K were collected using a liquid-nitrogen bath, and Brunauer–Emmett-Teller (BET) surface areas were calculated from data in the relative pressure range 0.05–0.30 P/P_0. Total pore volumes were taken near 0.99 P/P_0, whereas the micropore volume was obtained at 0.10 P/P_0. Pore size distributions and associated pore volumes were evaluated using the non-local density functional theory (NL-DFT) slit-pore model for carbon materials.

Oxygen Reduction Reaction:

The ORR activity of the catalysts was evaluated using a three-electrode configuration on a CHI 7091E electrochemical workstation (CH Instruments, USA). A rotating disk electrode (RDE, glassy carbon, 5 mm diameter; ALS, Japan) coated with the catalyst served as the working electrode, while a graphite rod (6 mm diameter) and an Ag/AgCl (3 M KCl) electrode were used as the counter and reference electrodes, respectively. To prepare the catalyst ink, 5 mg of catalyst was ultrasonically dispersed for 45 minutes in a mixture of isopropanol and water (1:1, 490 µL) along with 10 µL of 5 wt% Nafion to obtain a uniform suspension. Then, 10 µL of this ink was drop-cast onto the glassy carbon electrode and allowed to dry at room temperature, giving a catalyst loading of approximately 0.51 mg cm^{-2}. For comparison, commercial Pt/C (20 wt%, Sigma-Aldrich) was prepared and applied following the same procedure. All potentials were converted to the reversible hydrogen electrode (RHE) scale using the Nernst equation.

$$E_{RHE} = E_{Ag/AgCl} + 0.198\ V + 0.0591 \times pH \quad (1)$$

The electron transfer number per oxygen molecule was determined by using Koutechey-Levich (K-L) equation as follows: [S1]

$$\frac{1}{j} = \frac{1}{J_K} + \frac{1}{J_L} = \frac{1}{J_K} + \frac{1}{B\,\omega^{1/2}} \quad (2)$$

$$B = 0.62\, nFC_0(D_0)^{2/3}\nu^{-1/6} \quad (3)$$

$$J_k = nFKC_0 \quad (4)$$

Where j, J_k and J_L are measured , kinetic and diffusion current densities, ω is the angular velocity ($\omega = 2\Pi N$, N is the linear rotation speed) , n is the number of electron transfer, F is the faraday constant (96500 C mol^{-1}) , C_0 is the bulk concentration of O_2 (1.2×10^{-6} mol cm^{-3}) , D_0 is the diffusion coefficient of O_2 (1.9×10^{-5} cm^2 s^{-1}) , ν is the kinetic viscosity of electrolyte (0.01 cm^2 s^{-1}) and K is the electron transfer rate constant. Rotating ring-disk electrode (RRDE) measurements were carried out at a scan rate of 5 mV s^{-1} over the same potential window used for the RDE experiments. The RRDE assembly featured a 5 mm glassy carbon disk paired with a platinum ring as the working electrode. From the RRDE data, the electron transfer number (n) and the percentage of H_2O_2 produced were determined using the equations shown below. [S2]

$$n = \frac{4 \times I_D}{I_D + \frac{I_R}{N}} \quad (5)$$

$$H_2O_2\,(\%) = \frac{200 \times \frac{I_R}{N}}{I_D + \frac{I_R}{N}} \quad (6)$$

Here, I_D represents the disk current, I_R denotes the ring current, and N is the ring collection efficiency, supplied by the manufacturer (N = 0.37).

Zinc-Air battery:

The aqueous ZAB was assembled using polished zinc foil (100 µm thick, MTI Corporation) as the anode, a gas diffusion layer coated with catalyst as the cathode, a Celgard 5550 membrane as the separator, and 6 M KOH as the electrolyte. For the rechargeable cell, a 6 M KOH solution containing 0.2 M zinc acetate was utilized. The catalyst ink was prepared by dispersing 10 mg of the active material in a mixture of isopropanol and water (0.5 mL, 1:1 v/v), along with 10 µL of 5 wt% Nafion solution to form a uniform suspension. The mixture was sonicated for 30 min to obtain a homogeneous ink. Subsequently, the required amount of catalyst ink was drop-cast onto a 1 cm² gas diffusion layer, resulting in a catalyst loading of 3 mg cm^{-2}. For comparison, commercial Pt/C (20 wt%, Sigma-Aldrich) was also employed as a reference catalyst. All measurements were carried out using a Biologic BCS-805 battery cycler. The specific capacity of the ZAB was calculated using the following equations: [S1]

$$\text{Specific capacity (mAh g}^{-1}) = \frac{I \times t}{W_m} \quad (7)$$

where I is the applied current (mA), t is total serving time (hour), W_m is the mass of Zinc consumed in gram respectively.

Hydrogen evolution reaction:

A catalyst coated glassy carbon RDE was served as the working electrode, Pt sheet as the counter electrode, Ag/AgCl (3M KCl) as the reference electrode and 0.5 M H_2SO_4 as the electrolyte solution respectively for HER measurements. To obtain a uniform catalyst ink, 5 mg of catalyst powder was ultrasonically dispersed for 45 minutes in a solvent mixture consisting of isopropanol and water (2:1, 480 µL) together with 20 µL of a 5 wt% Nafion

solution. After homogenization, 7 μL of the resulting dispersion was dropped onto the surface of a GC electrode and allowed to dry naturally at room temperature, giving a final catalyst loading of approximately 0.35 mg cm^{-2}. For reference measurements, a Pt/C (20 wt%) ink was prepared following the identical protocol. Linear sweep voltammetry (LSV) was conducted at a rotation rate of 1600 rpm and a scan speed of 5 mV s^{-1}. The electrochemical surface area (ECSA) was determined from the double-layer capacitance (C_{dl}), which was obtained by recording cyclic voltammograms at different scan rates within the non-Faradaic potential window. The following equations was used to calculate the mass activity: [S3]

Mass activity (A g^{-1}) = $\frac{j}{m}$, where j is the measured current density at η = 0.35 V & m is the mass loading of the catalyst (0.35 mg cm^{-2})

Oxygen Evolution Reaction:

A catalyst ink was prepared by dispersing 5 mg of the catalyst in a mixture of isopropanol and water, followed by the addition of 50 μL of 5 wt% Nafion solution. The mixture was sonicated for 30 min to obtain a homogeneous ink. The resulting catalyst ink was then applied onto carbon cloth to achieve a loading of 1 mg cm^{-2} and subsequently dried under ambient conditions. Commercial RuO_2 was utilized as the benchmark catalyst. A graphite rod was employed as the counter electrode, while an Hg/HgO electrode served as the reference. Linear sweep voltammetry (LSV) measurements were carried out at a scan rate of 5 mV s^{-1}. The recorded potentials were converted to the reversible hydrogen electrode (RHE) scale using the equation:

$$E_{RHE} = E_{Hg/HgO} + 0.098\ V + 0.0591 \times pH. \quad (8)$$

Computational Details:

DFT calculations were performed in the linear combination of atomic orbitals (LCAO) method as implemented in Quantum ATK (Synopsys, USA) package.[S4] The exchange-correlation of electrons was included using Generalized Gradient Approximation (GGA) of Perdew-Burke Ernzerhof (PBE) correlation functional.[S5] The van der Waals interactions were taken care of using DFT-D2 of Grimme's method.[S6] Brillouin zone is sampled using a Monkhorst-Pack mesh of 2x2x1 k-points for all the geometry optimization and electronic structure calculations.4 The convergence criteria of 10^{-5} eV and 10^{-2} eV $Å^{-1}$ are used for the energy and forces, respectively, until all geometrical structures are totally relaxed. The experimental data at 298.15 K were taken from the NIST database for the gaseous molecules.

The ORR reaction pathways on the three models were systematically investigated.

In alkaline media, the four-electron ORR pathway could be summarized by the following elementary steps:

$$O_2\,(g) + H_2O\,(l) + * + e^- \rightarrow *OOH + OH^- \quad (9)$$

$$*OOH + e^- \rightarrow O* + OH^- \quad (10)$$

$$O* + H_2O + e^- \rightarrow OH* + OH^- \quad (11)$$

$$OH* + e^- \rightarrow OH^- + * \quad (12)$$

where the * denotes an active site of the catalyst, *OOH, *O and *OH are the oxygen-containing intermediates, respectively.

The free energies of reactants and each intermediate state at an applied electrode potential U were calculated as follows:

$$\Delta G = \Delta E + \Delta E_{ZPE} - T\Delta S - neU \quad (13)$$

where the ΔE, ΔE_{ZPE} and ΔS are the changes of total energy, zero-point energy and entropy during the reactions; T is the temperature; U is the electrode potential and n is the number of electrons transferred. The equilibrium potential U^0 for ORR was determined to be 0.455 V vs NHE alkaline media.

The Gibbs free energy of hydrogen adsorption (ΔG_{H*}) was evaluated according to:

$$\Delta G_{H*} = \Delta E_{ad} + \Delta E_{ZPE} - T\Delta S_H \quad (14)$$

where ΔE_{ad} denotes the adsorption energy of hydrogen, ΔE_{ZPE} is the zero-point energy correction, and ΔS_H represents the entropy change at temperature T.

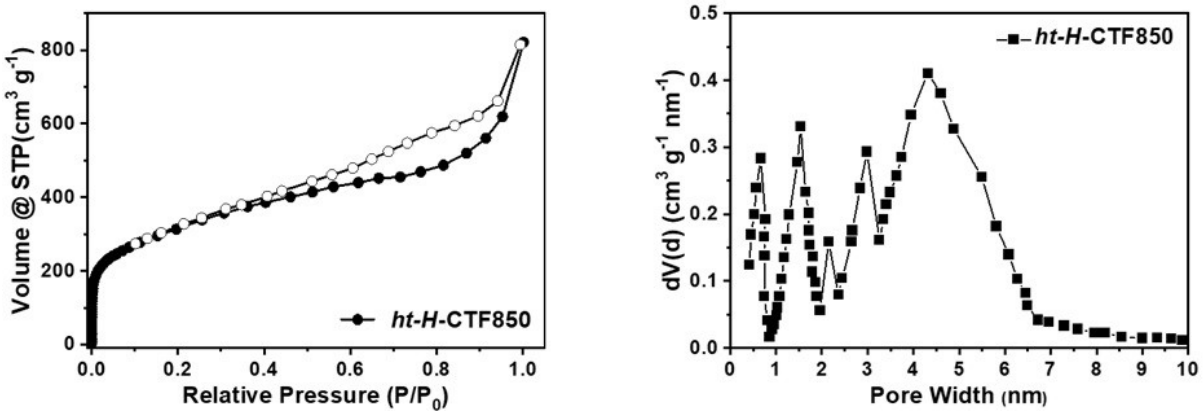

Figure S1: (a) BET Isotherm (inset sythetic scheme) and (b) Pore size distribution of *ht-H*-CTF850.

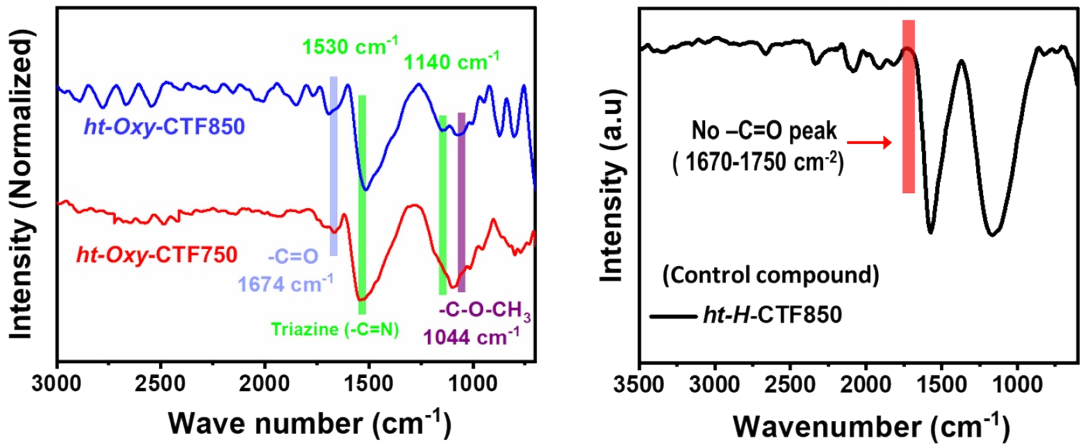

Figure S2: FTIR spectra *ht-Oxy*-CTFs (left) and *ht-H*-CTF850 (right).

Table S1: Textural properties for ***ht-H-CTF850*** (*control compound*) derived from N_2 isotherms (77 K, 1 bar).

Materials	**S_{BET} (m^2 g^{-1})**	**V_{micro} (cm^3 g^{-1})**	**V_{tot} (cm^3 g^{-1})**	**V_{micro}/V_{tot}**
***ht-H*-CTF850**	928	0.26	0.54	0.48

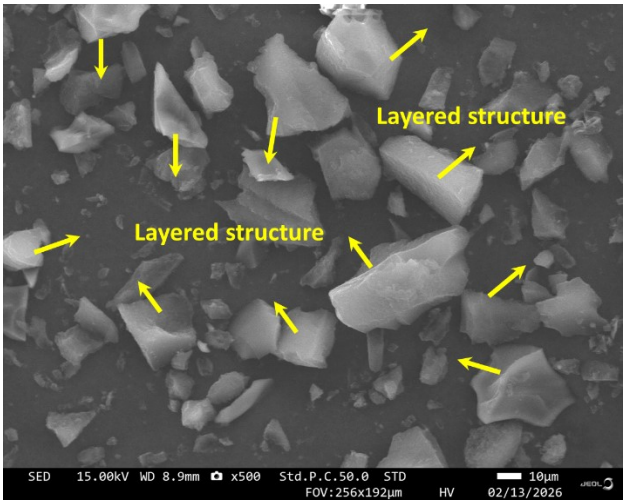

Figure S3: FESEM images illustrating the uniform layered morphology of *ht-Oxy*-CTF850 across multiple regions of the sample.

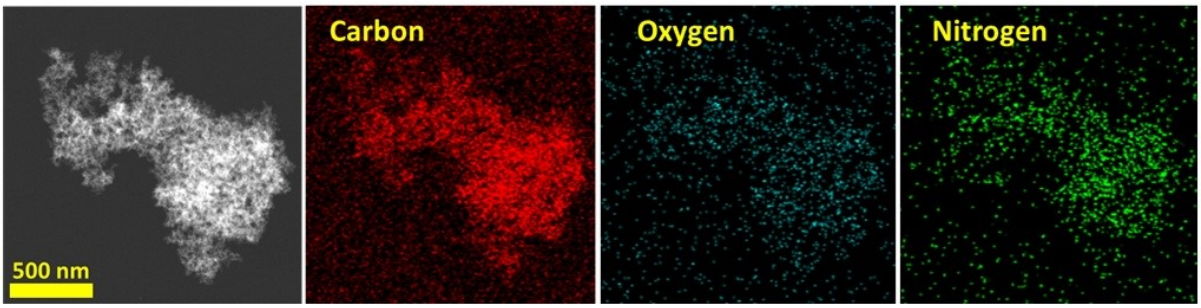

Figure S4: Energy-dispersive X-ray spectroscopy (EDX) elemental mapping of *ht-Oxy*-CTF750

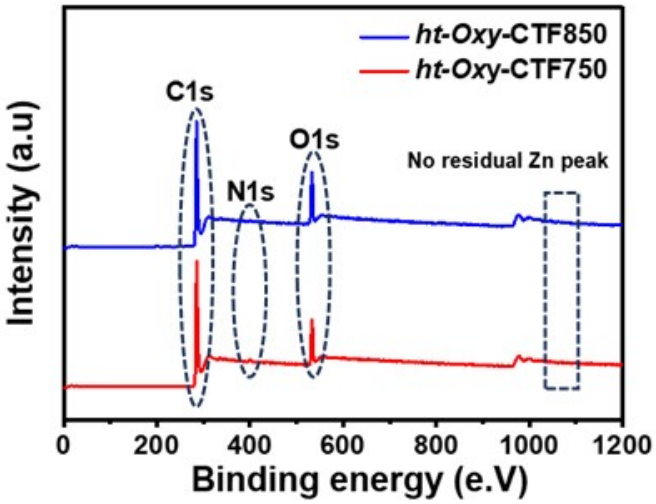

Figure S5: XPS survey spectrum of *ht-Oxy*-CTF750 and *ht-Oxy*-CTF850 respectively.

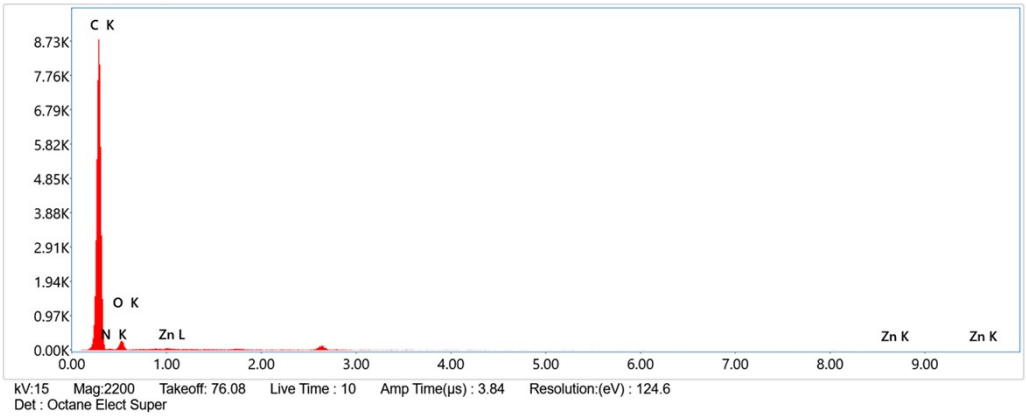

Figure S6: EDS spectrum of *ht-Oxy*-CTF850

Table S2: Zinc content in *ht-Oxy*-CTF samples determined by ICP-OES

Samples	Zinc concentration (ppm)
Blank (without sample)	0.01
***ht-Oxy*-CTF750**	3.72
***ht-Oxy*-CTF850**	5.33

Table S3: Atomic percentages of various elements, as determined by high-resolution core-level XPS analysis

Sample	**C (at%)**	**N(at%)**	**O(at%) ***
***ht-Oxy*-CTF750**	85.79	1.66	12.55
***ht-Oxy*-CTF850**	85.23	0.37	14.4

**Including moister/trapped oxygen contribution as seen in XPS analysis*

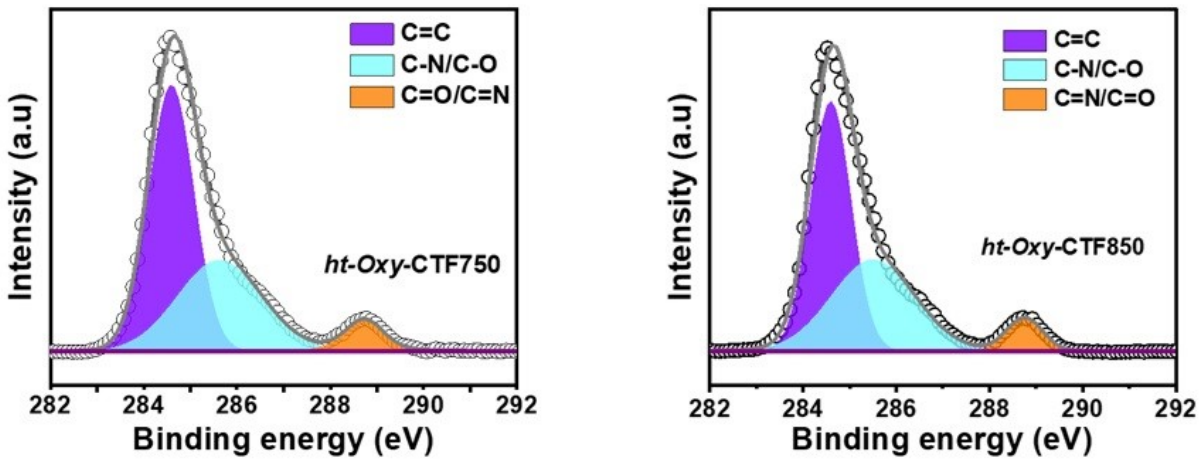

Figure S7: Deconvoluted XPS core-level spectra of C 1s: (a) *ht-Oxy*-CTF750 and (b) *ht-Oxy*-CTF850

Table S4: Relative percentages of different oxygen species determined by XPS analysis.

Materials	(-C-O) (%)	(-C=O) (%)	Trapped Moisture/gas (%)
***ht-Oxy*-CTF750**	54.76	3.03	42.21
***ht-Oxy*-CTF850**	48.55	2.66	48.79

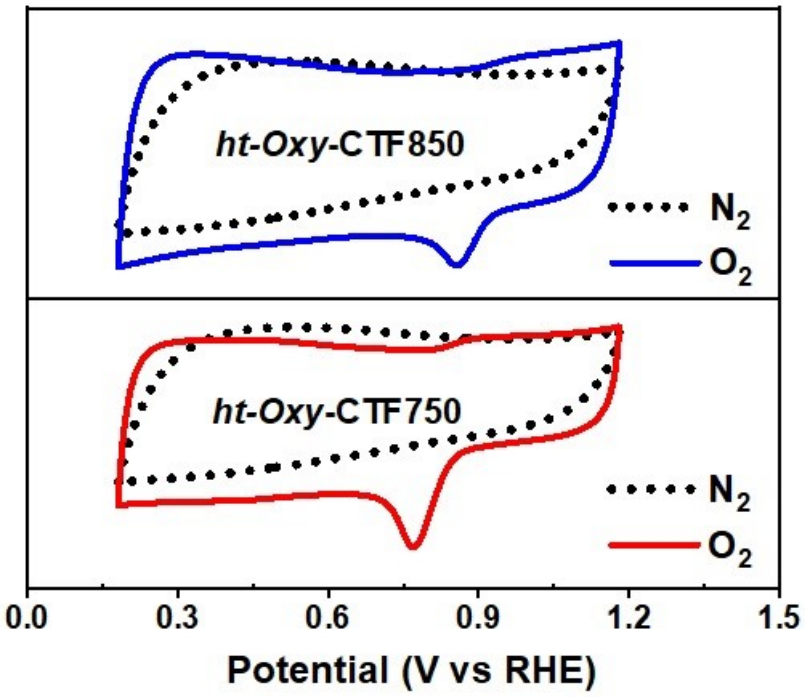

Figure S8: CV curves of *ht-Oxy*-CTFs in N_2-(dotted) and O_2-(solid) saturated 0.1M KOH electrolytes

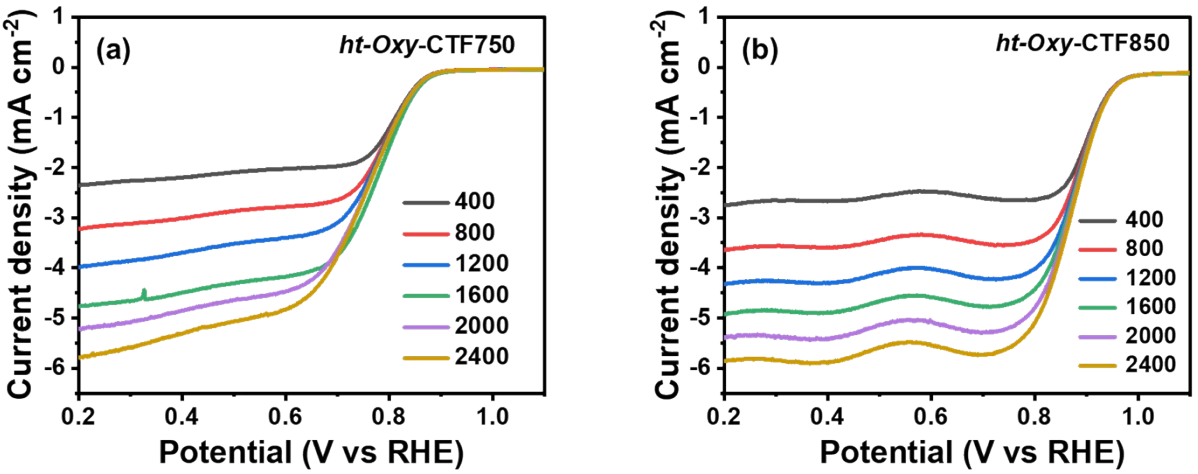

Figure S9: LSV curves of (a) *ht-Oxy*-CTF750 and (b) *ht-Oxy*-CTF850 at different rotation speed (400 - 2400 rpm).

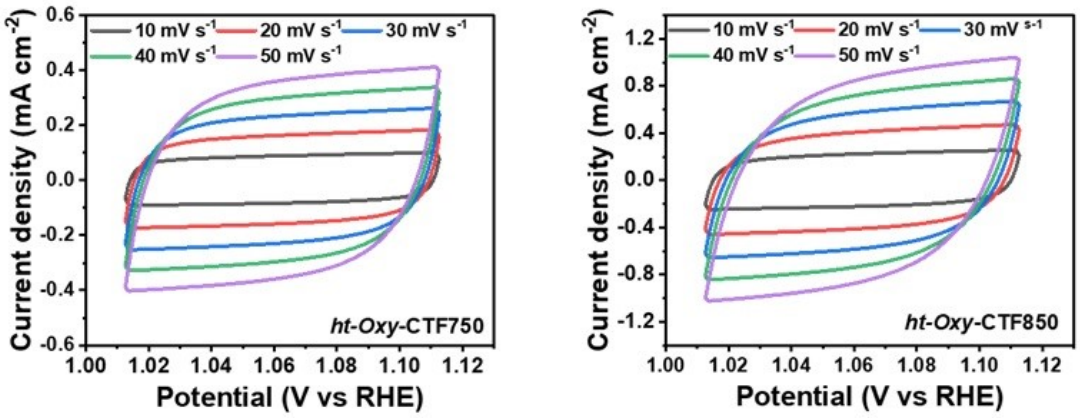

Figure S10: Cyclic voltammetry curves of *ht-Oxy*-CTFs in the non-faradic region at various scan rates. (a) *ht-Oxy*-CTF750 and (b) *ht-Oxy*-CTF850 in 0.1M KOH

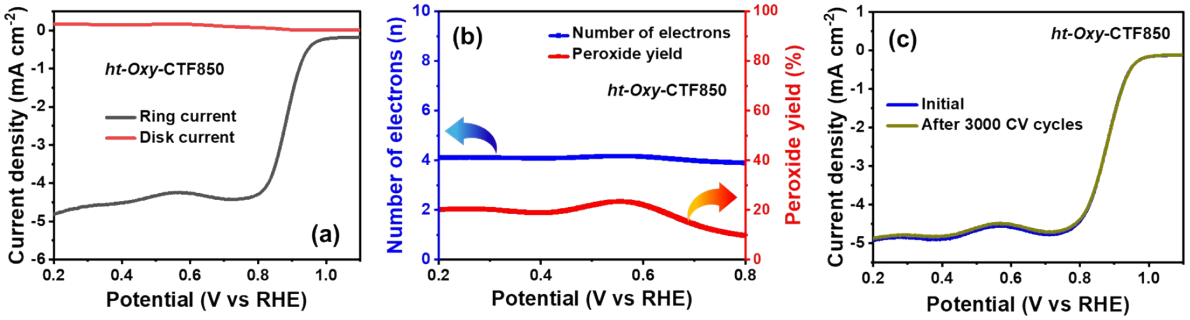

Figure S11: The ORR polarization curves of the *ht-Oxy*-CTF850 recorded on the RRDE at the rotation rate of 1600 rpm. (b) Electron transfer number(n) and H_2O_2 yield of *ht-Oxy*-CTF850 derived from RRDE measurements (0.2 - 0.8 V). (c) LSV curves of *ht-Oxy*-CTF850 before and after 3000 CV cycles.

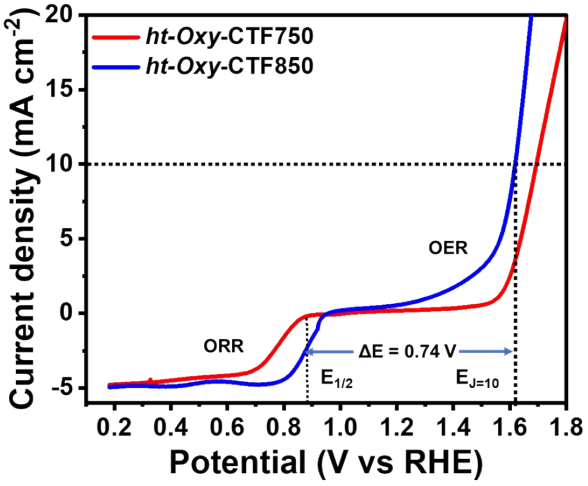

Figure S12: LSV curves between the ORR and OER *ht-Oxy*-CTF750 and *ht-Oxy*-CTF850.

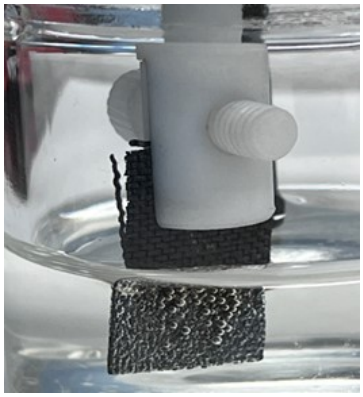

Figure S13: Photograph showing bubble formation on the electrode surface during the oxygen evolution reaction.

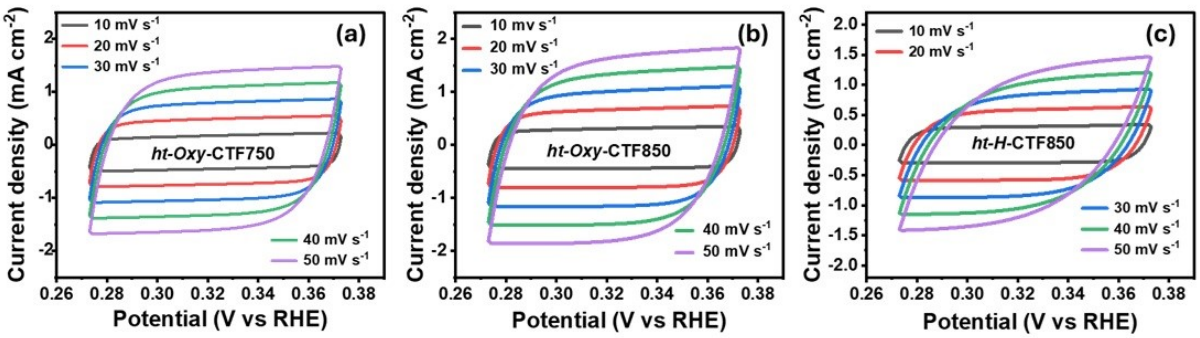

Figure S14: Cyclic voltammetry curves of *ht-Oxy*-CTFs in the non-faradic region at various scan rates. (a) *ht-Oxy*-CTF750 and (b) *ht-Oxy*-CTF850 and (c) *ht-H*-CTF850 in 0.5 H_2SO_4

Table S5: Calculated values of C_{dl}, ECSA, RF, mass activity, and specific activity of the synthesized catalysts.

Materials	**Electrolyte**	**C_{dl} (mF)**	**ECSA (cm^2)**	**RF**	**Mass activity at η @ 0.35 V (A g^{-1})**
***ht-Oxy*-CTF750**	0.5 H_2SO_4	5.68	162.2	827.5	114.2
***ht-Oxy*-CTF850**	0.5 H_2SO_4	6.46	184.5	941.3	166.2
ht-H*-CTF850** ***(control compound)	0.5 H_2SO_4	4.11	117.4	598.9	91.4

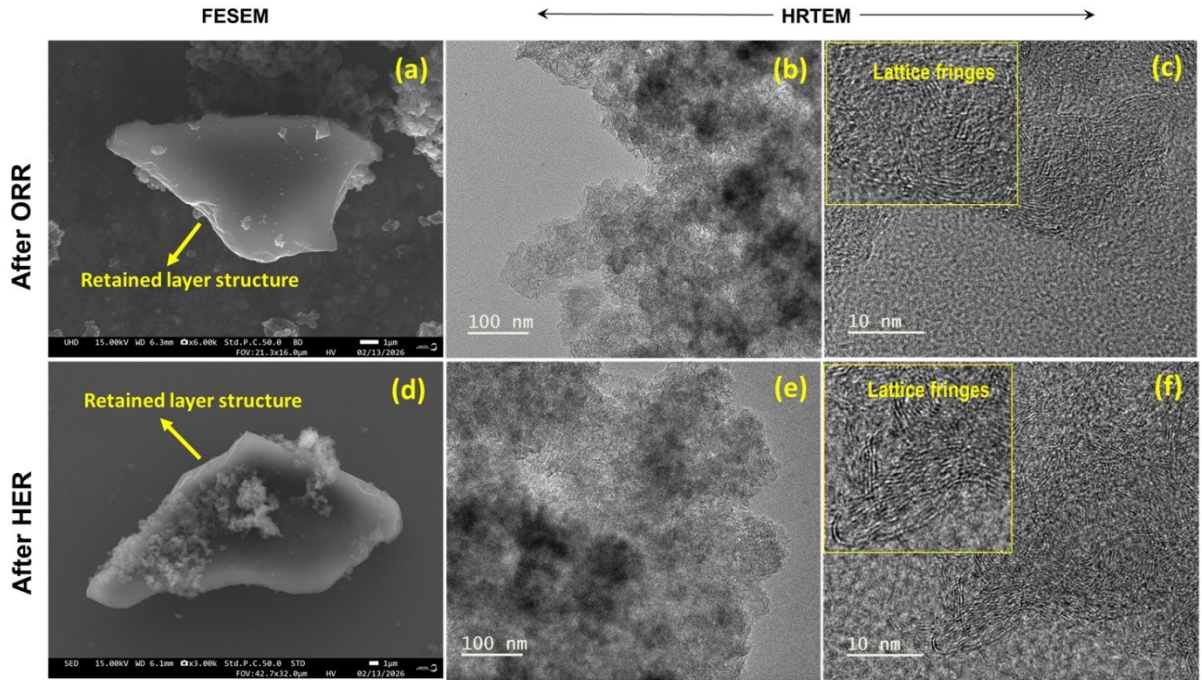

Figure S15: Morphological analysis of *ht-Oxy*-CTF850 after long term electrocatalytic stability test.

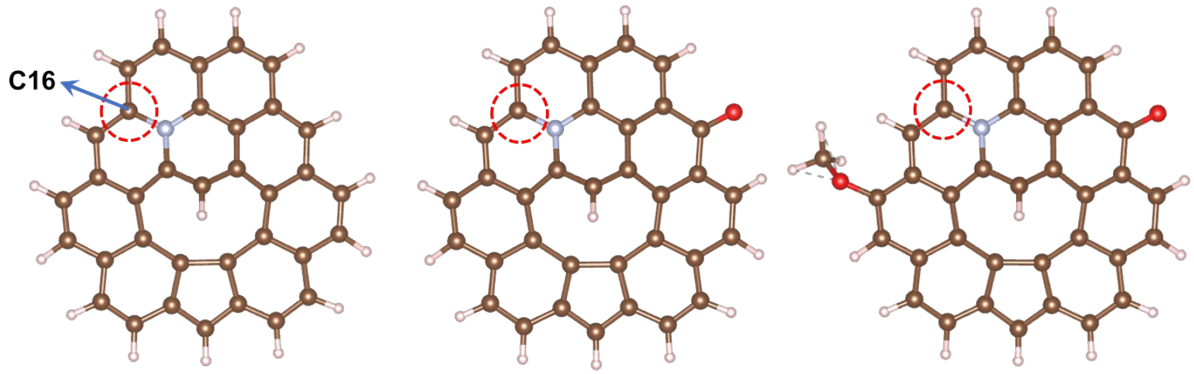

Figure S16: Optimized geometries of (a) Gr-N, (b) Gr-N+CO, and (c) Gr-N+CO+OMe.

Table S6: DFT-calculated partial charges (e) of individual carbon atoms in Gr–N, Gr–N+CO, and Gr–N+CO+OMe.

Carbon number	Gr-N	Gr-N+CO	Gr-N+CO+OMe
C1	-0.055	-0.039	-0.043
C2	0.135	0.137	0.136
C3	0.083	0.086	0.086
C5	0.03	0.032	0.031
C6	0.124	0.119	0.117
C7	0.018	0.029	0.03
C8	-0.022	0.129	0.127
C9	0.089	0.038	0.04
C10	0.101	0.031	0.025
C11	0.065	0.08	0.077
C12	0.005	0.003	-0.003
C13	-0.003	0.039	0.04

C14	0.01	0.009	0.01
C15	0.001	-0.001	-0.002
C16	0.17	0.171	0.173
C17	-0.048	-0.055	-0.055
C18	0.018	0.056	0.055
C19	-0.056	-0.06	-0.066
C20	0.036	0.036	0.032
C21	0.047	0.053	0.053
C22	-0.014	0.001	0
C23	-0.149	-0.155	-0.158
C24	-0.114	-0.145	-0.144
C25	0.151	0.151	0.15
C26	0.041	0.04	0.036
C27	0.108	0.112	0.11
C28	0.106	0.107	0.094
C33	0.147	0.145	0.144
C34	0.111	0.11	0.06
C35	0.012	-0.001	0.002
C37	-0.045	-0.023	-0.027
C39	0.035	0.033	0.03
C40	0.045	0.05	0.049
C42	0.046	0.053	0.025

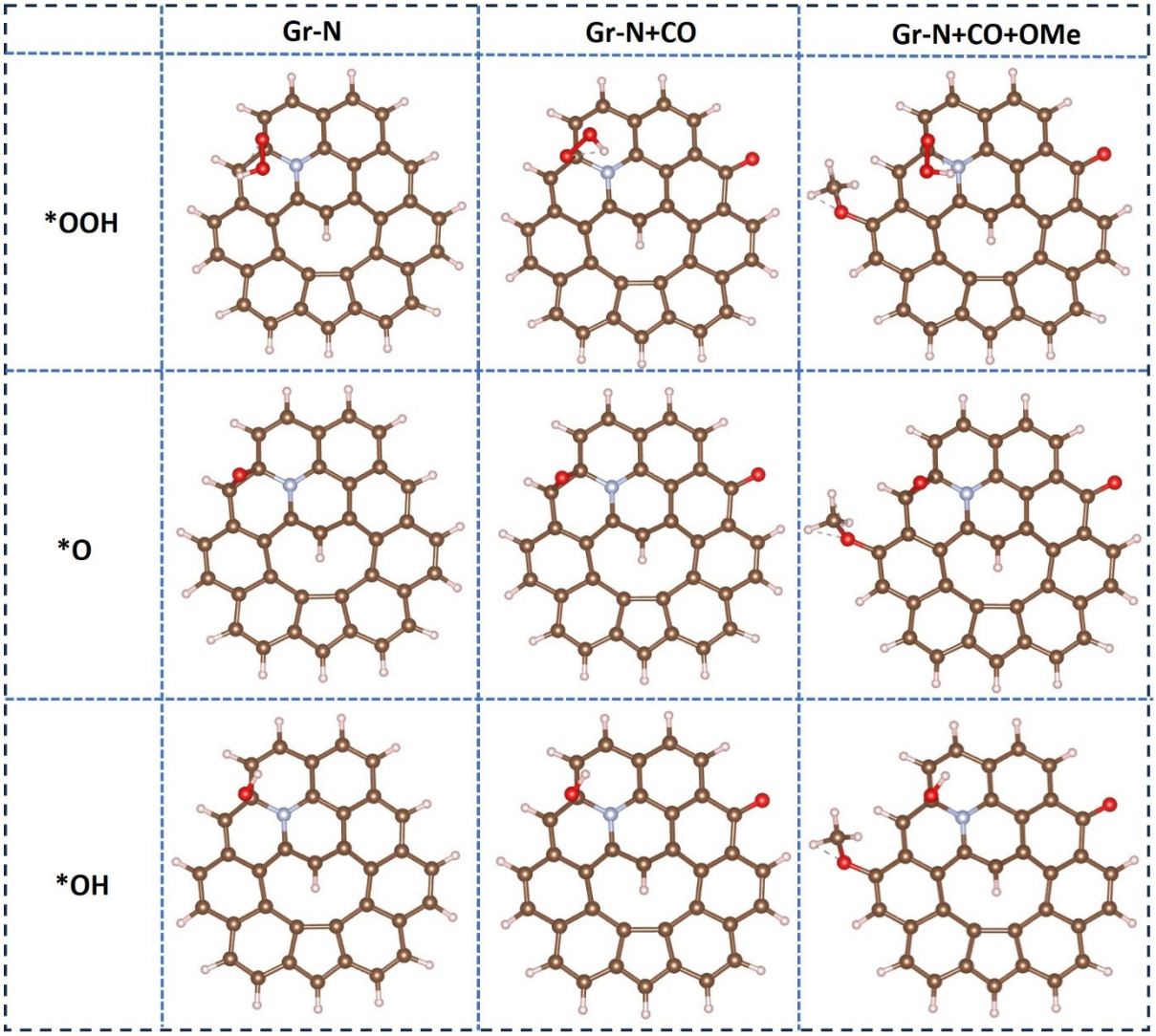

Figure S17: Optimized intermediate structures of the systems for each reaction step of ORR

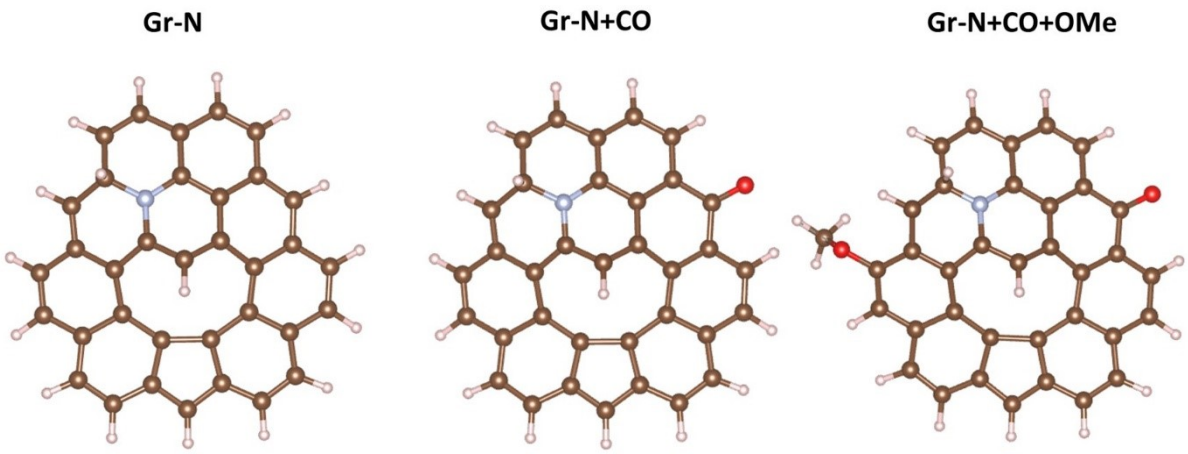

Figure S18: Optimized intermediate structures of the systems for HER

Table S7: Comparison of the Electrocatalytic ORR Activity of the *ht-Oxy*-CTF850 Catalyst with Other recently reported metal free carbon-based materials.

Catalysts	**Electrolyte**	**$E_{1/2}$ (V vs RHE)**	**Electron transfer number (n)**	**Reference**
***ht-Oxy*-CTF850**	**0.1 M KOH**	**0.88**	**~ 4**	**This work**
N-PCNFs-43.5	0.1 M KOH	0.85	3.90	*J. Mater. Chem. A*, 2025,**13**, 2650-2657
v-N/CNS/Gr	0.1 M KOH	0.85	3.93	*ACS Nano,* 2025, **19**, 31870−31881
N/S-CNH-900	0.1 M KOH	0.86	~ 4	*Small* 2025, **21**, 2410619
PD-COF-OH	0.1 M KOH	0.76	3.8	*Angew. Chem. Int. Ed.,* 2025, **64**, e202503434
NPS-HPCNF	0.1 M KOH	0.86	~ 4	*Adv. Energy Mater*. 2025, **15**, 2405236
Belt2	0.1 M KOH	0.84	3.97	*ACS Appl. Mater. Interfaces* 2025, **17**, 20096−20104
JUC-650	0.1 M KOH	0.72	3.86	*Small,* 2024**,** *20*, 2305759
dFCMC	0.1 M KOH	0.83	4.01	*Adv. Energy Mater*., 2024, **14**, 2401008
DAF-COF	0.1 M KOH	0.74	3.88	*Adv. Mater*., 2023, **35**, 2209129.
PYTA-PB-COF	0.1 M KOH	0.78	3.7	*Angew. Chem. Int. Ed.,* 2024, **63**, e202319247
VP/CNs	0.1 M KOH	0.86	3.98-4.0	*J. Am. Chem. Soc*., 2023, **145**,

				25695−25704
BUCT-COF-11/CNT	0.1 M KOH	0.72	3.98	*Angew. Chem. Int. Ed.,* 2023, **62**, e202216751
CMP-Tdz/CCA	0.1 M KOH	0.77	3.94	*Small* 2023, **19**, 2207298.
JUC-528	0.1 M KOH	0.7	3.81	*J. Am. Chem. Soc*., 2020, **142**, 8104−8108
NPF-CNS-2	0.1 M KOH	0.81	3.90	*Small* 2020, **16**, 2004342

Table S8: Comparison of zinc-air battery performance of the as-obtained ***ht-Oxy*-CTF850** catalyst with other previously reported metal free carbon-based catalyst.

Catalysts	**OCP (V)**	**Specific Capacity (mAh g^{-1}@mA cm^{-2})**	**Power density (mW cm^{-2})**	**Cyclic stability mA cm^{-2}@hr**	**Reference**
***ht-Oxy*-CTF850**	**1.46**	**792@10**	**132.2**	**5@205**	**This Work**
PD-COF-OH	1.35	676@10	111.6	ND	*Angew. Chem. Int. Ed*., 2025, **64**, e202503434
N/S-CNH-900	1.48	780@10	128	ND	*Small,* 2025, **21**, 2410619
JUC-650	1.38	722.6@50	101.5	ND	*Small,* 2024, **20**, 2305759.
FBNC-950	1.47	ND	147	5@100	*Carbon,* 2024, **225**, 119125.
NPCNF-O	1.46	726@10	125.1	5@200	*ACS Catal*., 2022, **12**, 4002−4015.
NPF@CNF80	1.49	804 @10	159	5@135	*ACS Appl. Mater. Interfaces*., 2021, **13**, 13328-13337.
NCF	1.41	ND	173	5 @10000 s	*Adv. Funct. Mater.,* 2021, **31**, 2103187.
CF-K-A	1.4	ND	61.5	ND	*Small,* 2018, **14**, 1800563
NPCS-900	1.4	684 @2	79	2@56	*Nano Energy*, 2019, **60**, 536–544.

NOGB-800	1.5	ND	111.9	10@30	*Adv. Energy Mater*., 2019, **9**, 1803867.
NDGs-800	1.45	750.8@10	115.2	10@78	*ACS Energy Lett*., 2018, **3**, 1183−1191.

ND: Not determined

Table S9: Comparison of the Electrocatalytic HER Activity of the *ht-Oxy*-CTF850 Catalyst with Other recently reported metal free carbon-based materials in acidic medium.

Catalysts	Electrolyte	Overpotential (mV)@ 10 mA cm^{-2}	Reference
***ht-Oxy*-CTF850**	**0.5 M H_2SO_4**	**81.5**	**This Work**
ED-COF	0.5 M H_2SO_4	103.6	*Adv. Sci*. 2025, **12**, 2501442
TPA-OMe	0.5 M H_2SO_4	353	*Small*, 2025, **21**, 2500502
WCMG	0.5 M H_2SO_4	179	*Carbon,* 2025, **224**, 120706
TAT-TFBE	0.5 M H_2SO_4	222	*Adv. Mater.* 2024, **36**, 2209919
BQ–BO	0.5 M H_2SO_4	230	*J. Mater. Chem. A*, 2024, **12**,3294–3303
PCTF-10500	0.5 M H_2SO_4	227	*ACS Appl. Nano Mater*. 2023, **6**, 24, 22684–22692
JLNU-302	0.5 M H_2SO_4	151	*J. Mater. Chem. A,* 2022, **10**, 10092–10097
4%-SPCNF	0.5 M H_2SO_4	310.8	*ACS Appl. Mater. Interfaces* 2022, **14**, 834−849
rGO/SiO_2	0.5 M H_2SO_4	134	*Small Methods*, 2021, **5**, 2100621.
Functionalized CNT	0.5 M H_2SO_4	135	*Nanoscale*, 2021, **13**, 4444–4450
FL-BP@BG	0.5 M H_2SO_4	385.9	*J. Mater. Chem. A*, 2020, **8**, 20446–20452
BINOL-CTF-10 500	0.5 M H_2SO_4	311	*ACS Appl. Mater. Interfaces* 2020, **12**, 44689−44699.
N, S,P Porous carbon	0.5 M H_2SO_4	260	*Carbon*, 2020, **162**, 586–594.

P, B-G	0.5 M H_2SO_4	385.9	*J. Mater. Chem. A*, 2020, **8**, 20446–20452.
N-carbon nanosheets	0.5 M H_2SO_4	90	*Energy Environ. Sci*., 2019, **12**, 322 333.
N, S-G	0.5 M H_2SO_4	230	*Angew. Chem., Int. Ed.,* 2018, **57**, 13302–13307.

References:

S1. F. Kong, X. Cui, Y. Huang, H. Yao, Y. Chen, H. Tian, G. Meng, C. Chen, Z. Chang and J. Shi, *Angew Chem. Int. Ed*. 2022, **61**, e202116290.

S2. Y. Zheng, H. Song, S. Chen, X. Yu, J. Zhu, J. Xu, K. A. I. Zhang, C. Zhang and T. Liu, *Small*, 2020, **16**, 2004342.

S3. M. Gao, W. Sheng, Z. Zhuang, Q. Fang, S. Gu, J. Jiang and Y. Yan, *J. Am Chem. Soc.,* 2014, **136**, 7077.

S4. S. Smidstrup, T. Markussen, P. Vancraeyveld, J. Wellendorff, J. Schneider, T. Gunst, B. Verstichel, D. Stradi, P. A. Khomyakov, U. G. Vej-Hansen, M.-E. Lee, S. T. Chill, F. Rasmussen, G. Penazzi, F. Corsetti, A. Ojanperä, K. Jensen, M. L. N. Palsgaard, U. Martinez, A. Blom, M. Brandbyge and K. Stokbro, *J. Phys.: Condens. Matter*, 2020, **32**, 015901.

S5. J. P. Perdew, K. Burke and M. Ernzerhof, *Phys. Rev. Lett.,* 1996, **77**, 3865-3868.

S6. S. Grimme, *J. Comput. Chem.* 2006, **27**, 1787-1799.